



# Numerical study of gas purge in polymer electrolyte membrane fuel cell



Jing Ding<sup>a</sup>, Yu-Tong Mu<sup>a</sup>, Shuang Zhai<sup>b</sup>, Wen-Quan Tao<sup>a,\*</sup>

<sup>a</sup> Key Laboratory of Thermo-Fluid Science and Engineering of MOE, School of Energy and Power Engineering, Xi'an Jiaotong University, Xi'an, Shaanxi 710049, China

<sup>b</sup> SAIC Motor Corporation Limited, Shanghai 201804, China

## ARTICLE INFO

### Article history:

Received 3 May 2016

Received in revised form 12 July 2016

Accepted 13 July 2016

Available online 11 August 2016

### Keywords:

Gas purge

Polymer electrolyte membrane fuel cell

Purge protocols

## ABSTRACT

Gas purge for eliminating water from gas diffusion layer (GDL) and membrane is of great importance for polymer electrolyte membrane fuel cell (PEMFC) start-up at subfreezing temperature. A gas purge model was developed to investigate the water transport phenomenon in GDL and membrane. In simulations, hydrogen and air were used as purge streams in anode and cathode, respectively. Effects of purge conditions on gas purge were numerically studied. In addition to relative humidity, flow rate and temperature, the flow configuration of purge gases was studied for the first time. In order to improve purge performance, several purge protocols were proposed and discussed in detail with respect to purge effectiveness and energy saving.

© 2016 Elsevier Ltd. All rights reserved.

## 1. Introduction

Polymer electrolyte membrane fuel cell (PEMFC) is an energy conversion device which can directly convert the chemical energy of fuel into electric power through electrochemical reaction. PEMFC is a promising power source for portable device, transport and distributed generation with advantages of high efficiency, no pollution and low noise [1]. In the past decades, much attention has been posed on the development of fuel cell vehicles. In the regard of fuel cell vehicles, successful and rapid start-up of fuel cell at sub-zero temperature, also called cold start, is of a great importance for their commercialization in automobile [2]. During operation, water is produced in cathode catalyst layer (CL) due to electrochemical reaction. When the membrane is fully hydrated, product water will resident in catalyst layer and formed ice or frost during cold start, which will block the catalyst layer and result in shutdown of fuel cell. If the membrane is rather dry, product water will diffuse into membrane and be stored there. In this case, the cell temperature may succeed to rise above 0 °C before the catalyst layer is totally blocked [3]. Therefore, every time a fuel cell is shut down, it is necessary to remove water in gas diffusion layer (GDL), catalyst layer and membrane by gas purge in order to create enough space for water storage during cold start.

Numerous studies have been reported on the experiments of gas purge. Tajiri et al. [4] developed a reproducible experimental method to characterize the drying process of gas purge by measuring the variation of high-frequency resistance (HFR). Ge and Wang

[5] measured the cell high-frequency resistance (HFR) during gas purge with different purge durations, and found that the cell HFR significantly influences the amount of cumulative product water in isothermal cold start. Lee et al. [6] developed a consistent and repeatable experimental method to determine local water content by using micro sensors to measure local HFR, and investigated water transport phenomena during gas purge in fuel cells. Lee et al. [7] developed a method for measuring the amount of residual water in the fuel cell, and use this method as well as HFR measurement to investigate the water removal characteristics. Sinha et al. [8] employed X-ray microtomography to quantify liquid water distribution in the gas diffusion layer and calculated the water removal rate with purge time at room temperature. St-Pierre et al. [9] developed a residence time distribution method and demonstrated its capability for detecting liquid water in gas channel and electrode. Cho and Mench [10] developed a special test system to investigate the fundamental behavior of evaporative water removal from diffusion media (DM) during gas purge with minimal in-plane gradients in saturation temperature. Based on the experimental results, they further developed a generic plot of purge efficiency, and proposed a purge protocol that applied composite flow rates of purge gas to enhance durability and reduce parasitic energy losses. Cho and Mench [11] also studied the effects of material properties, such as polytetrafluoroethylene (PTFE) content and geometric pore structure, on evaporative water removal from diffusion media, and compared the effects of phase-change-induced (PCI) flow and capillary flow on water removal. They also developed new methods to measure internal liquid flow rate and irreducible saturation. With ex situ test methods developed in [10,11] and neutron radiography (NR), Cho and Mench [12]

\* Corresponding author.

E-mail address: [wqtao@mail.xjtu.edu.cn](mailto:wqtao@mail.xjtu.edu.cn) (W.-Q. Tao).

**Nomenclature***Latin characters*

<i>a</i>	water activity [-]
<i>A</i>	area [m <sup>2</sup> ]
<i>C</i>	concentration [mol m <sup>-3</sup> ]
<i>D</i>	diffusivity [m <sup>2</sup> s <sup>-1</sup> ]
<i>EW</i>	equivalent weight [kg mol <sup>-1</sup> ]
<i>f</i>	volume fraction of water in the membrane [-]
<i>k</i>	mass transfer coefficient [m s <sup>-1</sup> ]
<i>L</i>	length [m]
<i>M</i>	molecule weight [kg mol <sup>-1</sup> ]
<i>n</i>	Bruggemann factor [-]
<i>P</i>	pressure [Pa]
<i>R</i>	resistance or universal gas constant [Ω] or [J K <sup>-1</sup> mol <sup>-1</sup> ]
<i>s</i>	saturation [-]
<i>S</i>	source term [s <sup>-1</sup> ]
<i>t</i>	time [s]
<i>T</i>	temperature [K]
<i>V</i>	molar volume [m <sup>3</sup> mol <sup>-1</sup> ]
<i>w</i>	width [m]
<i>x</i>	distance away from cathode inlet [m]

*Greek characters*

$\delta$	depth [m]
$\varepsilon$	porosity or volume fraction [-]
$\kappa$	electrical conductivity [S m <sup>-1</sup> ]
$\lambda$	water content [-]
$\rho$	density [kg m <sup>-3</sup> ]
$\phi$	relative humidity [-]

*Subscripts and superscripts*

0	initial value
a	anode
air	air
avg	average value
c	cathode
cell	fuel cell
chan	channel
CL	catalyst layer
d	desorption
dry	dry membrane
eff	effective value
eq	equivalent value
g	purge gas
GDL	gas diffusion layer
H <sub>2</sub>	hydrogen
H <sub>2</sub> O	water
l	liquid water
land	land
m	ionomer
mem	membrane
o	reference value
sat	saturated water vapor
total	total value
V	volume
w	water
air	relative humidity
$\phi$	relative humidity [-]

investigated the coupled effects of land to channel width ratios and diffusion media (DM) structure on the evaporative water removal during gas purge. Tang et al. [13] used in situ neutron imaging to investigate the gas purge performance for different wettability of flow channel, and found that super-hydrophilic coating on the landings and super-hydrophobic coating on the channels helped to improve water removal. Owejan et al. [14] investigated water transport in PEMFC by using ex situ and in situ experiments and proposed a one-dimensional model to calculate the effectiveness of cathode purge for water removal based on the experimental results.

It is also important to study effective purge methods. Kim et al. [15] proposed a new purge method that added a small amount of hydrogen into the dry air. Due to the hydrogen–oxygen catalytic reaction, a large amount of heat was generated, which facilitated water evaporation in CL and GDL. Kim et al. [16] proposed a new and more effective purge method that used a sudden pressure reduction to remove residual water in membrane electrode assembly (MEA) and GDL, and verified the purge performance via several techniques, including cold start experiments and durability tests.

Since numerical simulations can provide information that is difficult to obtain from experiments, much efforts have been devoted to the development of gas purge models. Sinha and Wang [17] proposed an analytical purge model to describe the GDL drying and membrane drying process in the cathode, and provided fundamental insight into gas purge phenomena. The predicted results were verified through tomographic experiments. Based on the analytical model presented by Sinha and Wang [17], Ito et al. [18] developed a modified model to investigate the water removal behavior in GDL and membrane during preswitching gas purge for unitized reversible fuel cells (URFCs). Sinha and Wang [19] developed a more

comprehensive three-dimensional two-phase transient gas purge model. The model accounted for capillary transport of liquid water, vapor diffusion, and water transport between anode and cathode through the membrane. Khandelwal et al. [20] developed a transient two-phase computational model to describe water redistribution in PEMFC after shutdown, which for the first time included thermo-osmotic flow in the electrolyte membrane and phase-change induced (PCI) flow in the porous media, and investigated impacts of thermo-osmotic, capillary and PCI flow on water removal. Wang et al. [21] developed a dynamic three-phase transport model to study water uptake and transport process in PEMFC during cold start and shutdown. They ran simulation to analyze the purge time and energy consumption as a function of initial stack temperature and saturation level of GDL for drying the membrane to a target level during shutdown.

In the relevant literature, nitrogen was usually used as purge gas in research on gas purge or cold start, as reported in [4,5,7,11–14,17–19,22–25]. However, an additional gas tank and pipes are required for nitrogen gas purge, which will definitely increase the complexity and the weight of the fuel cell system. As a result, the cost of the fuel cell vehicle may increase whereas the cruising range may decrease. In comparison, gas purge with hydrogen in the anode and air in the cathode is a better choice, because no extra device is required. However, research on gas purge with hydrogen and air is scarce [15,16]. Therefore, the gas purge process using hydrogen and air is investigated in this work.

The purge model presented by Sinha and Wang [17] and Ito et al. [18] considered only cathode purge. In this study, we further developed their model to predict gas purge process for both anode and cathode and water transport through the membrane. To validate our model, numerical predictions of HFR vs purge time are

compared with experimental results. Based on our model, parametric effects of purge conditions on gas purge in the PEMFC designed by SAIC are investigated. Furthermore, several purge protocols are also discussed with respect to purge effectiveness and energy consumption for the optimization of gas purge.

## 2. Gas purge model

Once purge gas is introduced in the gas channel, liquid water in the flow channel is swept out immediately. Then, water in GDL begins to be removed through evaporation. GDL drying can be described by an evaporation front moving forward through GDL, as shown in Fig. 1. Liquid water evaporates at the evaporation front. Then, water vapor diffuses into flow channel and is carried away by the purge gas. After GDL drying is finished, water in CL pores and water absorbed by ionomers in CL and membrane start to be removed and the evaporation front penetrates into CL. Therefore, gas purge can be idealized as removal of liquid water in GDL followed by ionomer drying. For simplicity of analysis, we add volume of pores in CL to that in GDL to obtain an equivalent GDL thickness. Similarly, we add volume of ionomers in CL to that in membrane to obtain an equivalent membrane thickness. It is noted that the total mass of water remains the same before and after such simplification. The expressions of equivalent GDL thickness and equivalent membrane thickness are as follows:

$$\delta_{\text{GDL}}^{\text{eq}} = \delta_{\text{GDL}} + \frac{\varepsilon_{\text{CL}}}{\varepsilon} \delta_{\text{CL}} \quad (1)$$

$$\delta_{\text{mem}}^{\text{eq}} = \delta_{\text{mem}} + 2\varepsilon_{\text{m}} \delta_{\text{CL}} \quad (2)$$

where  $\delta_{\text{GDL}}$ ,  $\delta_{\text{CL}}$  and  $\delta_{\text{mem}}$  are the actual thickness of GDL, CL and membrane, respectively.  $\varepsilon$  and  $\varepsilon_{\text{CL}}$  denote the porosity of GDL and CL, respectively, while  $\varepsilon_{\text{m}}$  denotes the volume fraction of ionomer in CL. Actually, it is more difficult to remove water from CL than from GDL due to the smaller porosity of CL. Whereas, in our model, the CL was treated as a portion of GDL. As a result, the gas purge process would be faster than reality. However, the purge time for CL was much shorter than GDL since CL was much thinner than GDL. Therefore, the purge process would not be affected much by such simplification.

Therefore, the gas purge model can be divided into GDL drying model and membrane drying model. Apart from the above-mentioned simplification, there are also some assumptions which are the same as those in the models of [26,18]:

1. Velocity in flow channel is uniform and constant.
2. The temperature of purge gas is the same as the cell temperature.
3. Vapor transport in GDL is only driven by diffusion.

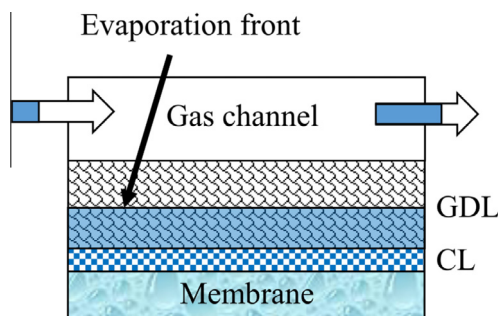


Fig. 1. Schematic representation of GDL drying.

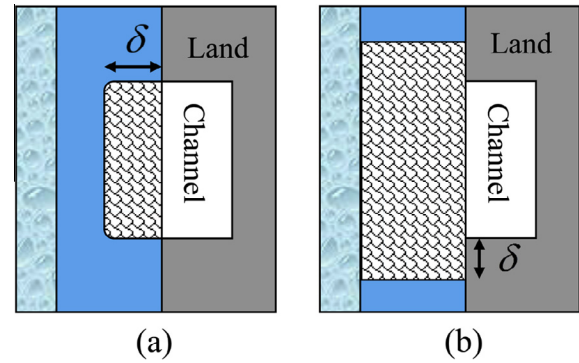


Fig. 2. Schematic representation of liquid water removal during (a) through-plane drying and (b) in-plane drying.

### 2.1. GDL drying model

According to the work of Sinha and Wang [17], GDL drying can be divided into three stages: through-plane drying, in-plane drying and vapor-phase transport, as shown in Fig. 2. In terms of through-plane drying, the evaporation front is at a distance of  $\delta$  away from the GDL-channel interface at any time instant  $t$ . The water conservation in the portion of GDL facing channel is given by

$$-D_g^{\text{w,eff}} \frac{\Delta C}{\delta} = \frac{d}{dt} \left[ (\delta_{\text{GDL}} - \delta) \frac{\varepsilon s_0 \rho_l}{M^{\text{H}_2\text{O}}} \right] \quad (3)$$

where  $\varepsilon$ ,  $s_0$  and  $\rho_l$  refer to porosity of GDL, initial saturation and liquid water density, respectively;  $M^{\text{H}_2\text{O}}$  is the molecular weight of water;  $D_g^{\text{w,eff}}$  is the effective diffusivity of water vapor in purge gas, which accounts for porosity and tortuosity of GDL [19] and the effects of pressure and temperature [27]

$$D_g^{\text{w,eff}} = D_g^{\text{w}} \varepsilon^n \left( \frac{P_0}{P} \right) \left( \frac{T}{T_0} \right)^{\frac{1}{n}} \quad (4)$$

where  $n$ ,  $P_0$  and  $T_0$  refer to the Bruggemann factor, reference pressure and reference temperature, respectively.  $P$  and  $T$  are operating pressure and temperature, respectively. The Bruggemann factor  $n$  is set as 2 in our model, the same value set by Sinha and Wang [17] and Ito et al. [18].

It is usually assumed that the water concentration at the evaporation front is equal to the saturated water vapor concentration. Hence, the concentration gradient can be expressed as

$$\Delta C = C_{\text{sat}}(1 - \phi) \quad (5)$$

where  $C_{\text{sat}}$  denotes the concentration of saturated water vapor and  $\phi$  denotes the relative humidity in the flow channel.

In addition to vapor diffusion toward gas channel, liquid water in GDL is also removed by water transport through membrane, which was not considered in the model presented by Sinha and Wang [17] and Ito et al. [18]. Assuming that water transport through the membrane only changes the water saturation behind the evaporation front, we can write the water balance equation in GDL as

$$\varepsilon(\delta_{\text{GDL}} - \delta) \rho_l \frac{\partial s_0}{\partial t} = -M^{\text{H}_2\text{O}} D_w^{\text{m}} \frac{\rho_{\text{dry}}}{EW} \frac{\lambda_c - \lambda_a}{\delta_{\text{mem}}} \quad (6)$$

where  $D_w^{\text{m}}$  is the diffusivity of water in ionomer, while  $\rho_{\text{dry}}$  and  $EW$  are the density and the equivalent weight of a dry membrane, respectively. Besides,  $\lambda_c$  and  $\lambda_a$  are water content at cathode and anode membrane surface, respectively.

During in-plane drying, there is only water vapor in the channel-facing GDL. Water removal is driven by vapor concentra-

tion gradient across the GDL. Assuming that vapor concentration is linearly distributed along the through-plane direction, the water balance equation in GDL portion facing channel can be given by

$$\frac{d}{dt} \left[ \frac{P_{\text{sat}}}{RT} \frac{(a_{\text{chan}} + \phi)}{2} \varepsilon \delta_{\text{GDL}} \right] = \frac{\rho_{\text{dry}}}{EW} k_d (\lambda_{\text{chan}} - \lambda_{\text{chan}}^{\text{eq}}) - D_g^{\text{w,eff}} \frac{P_{\text{sat}}}{RT} \times \frac{(a_{\text{chan}} - \phi)}{\delta_{\text{GDL}}} \quad (7)$$

where  $a_{\text{chan}}$  is the water activity at membrane surface facing channel,  $R$  is the universal gas constant and  $k_d$  is the mass transfer coefficient for desorption or absorption of water, which is calculated by [28]

$$k_d = \begin{cases} 4.59 \times 10^{-5} f_v \exp \left[ 2416 \left( \frac{1}{303} - \frac{1}{T} \right) \right], & \text{desorption} \\ 1.14 \times 10^{-5} f_v \exp \left[ 2416 \left( \frac{1}{303} - \frac{1}{T} \right) \right], & \text{absorption} \end{cases} \quad (8)$$

Here,  $f_v$  is the volume fraction of water in the electrolyte membrane and it is calculated by

$$f_v = \frac{\lambda V_w}{V_{\text{mem}} + \lambda V_w} \quad (9)$$

where  $V_w$  and  $V_{\text{mem}}$  are the molar volumes of water and a dry membrane, respectively. Besides,  $\lambda_{\text{chan}}$  is the actual water content at the membrane surface facing channel,  $\lambda_{\text{chan}}^{\text{eq}}$  is the equilibrium membrane water content which is evaluated by water activity  $a_{\text{chan}}$ . The first term in the right hand side of Eq. (7) accounts for the water flux into GDL due to membrane water desorption, which is assumed to be proportional to the difference between the local ionomer water content and its equilibrium sorption value [29].

The equilibrium water content of Nafion membrane as a function of water activity has been measured by Zawodzinski [30] and Hinatsu [31]. Their results showed that membrane water content in equilibrium with water vapor decreased with increasing temperature. They measured the equilibrium water content of a Nafion 117 membrane in contact with water vapor at 303 K and 353 K, respectively. The correlations between water content and water activity at 303 K [30] and 353 K [31] are:

$$\lambda_{303} = 0.043 + 17.81a - 39.85a^2 + 36.0a^3 \quad (10)$$

$$\lambda_{353} = 0.300 + 10.8a - 16.0a^2 + 14.1a^3 \quad (11)$$

In our model, we assume that water content is a function of temperature. The linear interpolation expression that was employed by Ge et al. [28] is adopted here

$$\lambda = \lambda_{303} + \frac{\lambda_{353} - \lambda_{303}}{50} (T - 303) \quad (12)$$

As for in-plane drying, the evaporation front penetrates into GDL portion facing land. The water balance equation in the land region of GDL can be written as

$$-D_g^{\text{w,eff}} \frac{C_{\text{sat}}(1 - \phi)}{\left[ \frac{\delta}{\delta_{\text{GDL}}} + \frac{2\delta_{\text{GDL}}}{w_{\text{land}}} \right] \delta_{\text{GDL}}} = \frac{d}{dt} \left[ \left( \frac{w_{\text{land}}}{2} - \delta \right) \frac{\varepsilon S_0 \rho_l}{M^{\text{H}_2\text{O}}} \right] \quad (13)$$

where  $w_{\text{land}}$  is the land width. For detailed derivation of the denominator in the left hand side, please refer to [17].

During vapor-phase transport, the land-facing GDL is filled only with water vapor. Similar to the water balance of GDL portion facing channel during in-plane drying, the water balance of land-facing GDL is computed by

$$\frac{d}{dt} \left[ \frac{P_{\text{sat}}}{RT} \frac{(a_{\text{land}} + \phi)}{2} \varepsilon \delta_{\text{GDL}} \right] = \frac{\rho_{\text{dry}}}{EW} k_d (\lambda_{\text{land}} - \lambda_{\text{land}}^{\text{eq}}) - D_g^{\text{w,eff}} \frac{P_{\text{sat}}}{RT} \times \frac{(a_{\text{land}} - \phi)}{\delta_{\text{eff}}} \quad (14)$$

where  $a_{\text{land}}$  is the water activity at the membrane surface facing land;  $\lambda_{\text{land}}$  and  $\lambda_{\text{land}}^{\text{eq}}$  are the actual water content at the membrane surface facing land and its equilibrium water content, respectively.  $\delta_{\text{eff}}$  is the effective diffusion distance from membrane surface facing land to gas channel, whose detailed derivation can be found in [17].

## 2.2. Membrane drying model

As for water content in the membrane, it can be calculated as follows:

$$\delta_{\text{mem}} \frac{\partial \lambda_{\text{avg}}}{\partial t} = k_{d,c} (\lambda_c^{\text{eq}} - \lambda_c) + k_{d,a} (\lambda_a^{\text{eq}} - \lambda_a) \quad (15)$$

where  $\lambda_{\text{avg}}$  is the average water content over the thickness of membrane;  $k_{d,c}$  and  $k_{d,a}$  are mass transfer coefficients for cathode and anode, respectively. Subscripts a and c denote anode and cathode, respectively. The first term and the second term in the right-hand side account for water desorption in the cathode side and anode side, respectively. Assuming that water content is linearly distributed along the membrane thickness, we can determine the average water content by

$$\lambda_{\text{avg}} = \frac{\lambda_c + \lambda_a}{2} \quad (16)$$

However, in the following two cases, special treatments should be carried out for mass transfer coefficients. For one case, if both cathode side and anode side of membrane are in contact with liquid water,  $k_{d,c}$  and  $k_{d,a}$  are assumed to be infinite because water content reaches its equilibrium quickly [30]. Hence, for this case, we have

$$\lambda_c = \lambda_c^{\text{eq}} \quad (17)$$

$$\lambda_a = \lambda_a^{\text{eq}} \quad (18)$$

Accordingly, water content of membrane can be expressed as

$$\lambda_{\text{avg}} = \frac{\lambda_c^{\text{eq}} + \lambda_a^{\text{eq}}}{2} \quad (19)$$

For the other case, if only one side of membrane is in contact with liquid water, the mass transfer coefficient of that side is assumed to be infinite. For example, if only cathode side of membrane is covered with liquid water,  $k_{d,c}$  is assumed to be infinite. Then, water content is given by

$$\delta_{\text{mem}} \frac{\partial \lambda_{\text{avg}}}{\partial t} = D_w^m \frac{\lambda_c^{\text{eq}} - \lambda_a}{\delta_{\text{mem}}} + k_{d,a} (\lambda_a^{\text{eq}} - \lambda_a) \quad (20)$$

Since drying conditions in GDL facing channel and land are different, water contents in the membrane portions facing channel and land differ from each other during gas purge. To account for different water content distribution in the in-plane direction, the membrane portions facing channel and land are treated separately. For simplicity, we assume that there is no in-plane water transport within the membrane. The average water content facing channel and land,  $\lambda_{\text{chan,avg}}$  and  $\lambda_{\text{land,avg}}$ , can be obtained by applying Eqs. (15)–(20) for membrane portions facing channel and land, respectively.

## 2.3. Relative humidity in flow channel

The governing equation of water vapor in the flow channel is given by [17]

$$\frac{\partial \phi}{\partial t} + u \frac{\partial \phi}{\partial x} = \frac{\partial}{\partial x} \left( D_g^w \frac{\partial \phi}{\partial x} \right) + S_\phi \quad (21)$$

where  $S_\phi$  is the source term which varies in different drying stages. Expressions of source term at different stages are listed in Table 1.

**Table 1**  
Source terms of relative humidity in flow channel for different stages.

Stage	$S_\phi$
Through-plane drying	$\frac{D_g^{w,eff}}{\delta_{chan}} \frac{1-\phi}{\delta}$
In-plane drying	$\frac{D_g^{w,eff}}{\delta_{chan}} \frac{1-\phi}{\delta} + \frac{D_g^{w,eff}}{\delta_{chan}} \frac{a_{chan}-\phi}{\delta_{GDL}}$
Vapor-phase transport	$\frac{D_g^{w,eff}}{\delta_{chan}} \frac{a_{chan}-\phi}{\delta_{GDL}} + \frac{D_g^{w,eff}}{\delta_{chan}} \frac{a_{land}-\phi}{\delta_{eff}}$

For the water vapor governing equation, the QUICK scheme is used for the discretization of the convective term, and the central difference scheme is chosen for the diffusion term. The source term is linearized in order to accelerate convergence. The time derivative is discretized using a backward difference scheme. Furthermore, the whole equation is evaluated in a fully implicit manner.

### 3. Validation

In order to validate our gas purge model, it is necessary to compare the predictions of our model with experimental results. HFR is used as an indicator of membrane hydration in the experiments of gas purge [4,5,23], because HFR and water content are uniquely related and the measurement of HFR is much easier than that of water content. To compare our numerical results with experimental results, we need to convert membrane water content into membrane HFR.

The electric conductivity of Nafion membrane is a function of membrane water content. Springer et al. [32] measured the electric conductivity of a Nafion 117 membrane and proposed a correlation between electric conductivity and membrane water content as follows

$$\kappa = (0.5139\lambda - 0.326) \exp \left[ 1268 \left( \frac{1}{303} - \frac{1}{T} \right) \right] \quad (22)$$

In this work, GORE-SELECT membrane was chosen in numerical simulation. Since GORE-SELECT membrane is microscopically reinforced, the proton electric conductivity has to be adjusted to approximately half of the value of an un-reinforced membrane [33]. Hence, it follows that

$$\kappa^{eff} = \frac{1}{2} \times \kappa = \frac{1}{2} \times (0.5139\lambda - 0.326) \exp \left[ 1268 \left( \frac{1}{303} - \frac{1}{T} \right) \right] \quad (23)$$

Once the membrane water content is obtained, the membrane resistance under channel and land for a small section  $dx$  can be determined by

$$R_i = \frac{\delta_{mem}}{\kappa^{eff}(\lambda_i) w_i dx}, \quad i = \text{chan, land} \quad (24)$$

Connecting all membrane resistance under channel and land in parallel, we can obtain the total membrane resistance  $R_{total}$ , which can be used to calculate the membrane HFR

$$\text{HFR} = R_{total} A_{mem} \quad (25)$$

where  $A_{mem}$  is the active area of the membrane.

Tajiri et al. [4] measured the cell HFR during gas purge under various purge conditions. Our simulations were conducted in the same conditions as those of the experiments in [4]. Fig. 3 plots the variations of changes in HFR for simulations and experiments with purge time at different flow rates of purge gas. Generally speaking, the simulation results are in good agreement with the experimental results. The discrepancy between the simulated curves and the experimental curves can be attributed to the following two reasons. For one thing, in-plane transport of water in GDL and membrane was not considered in our model. Although

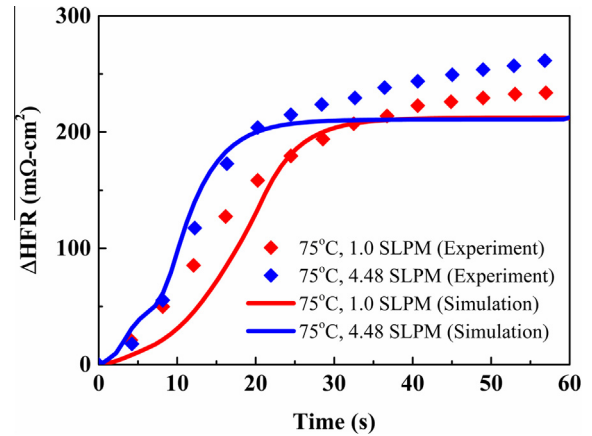


**Fig. 3.** Variation of changes in membrane HFR with time for 75 °C cell temperature (squares – experimental results; solid lines – simulation results).

the HFR of channel area and rib area showed great difference in the experiments of Lee et al. [6], which indicated that in-plane water transport within the membrane was much slower than water removal rate during gas purge, in-plane water transport within the membrane still has certain effect on the variation of HFR. For another, the evaporation process at the evaporation front was simplified by vapor diffusion. A more sophisticated evaporation mechanism, such as water phase change functions adopted by Jiao and Li [34], can be applied to further improve the model in the future.

### 4. Results and discussion

Our model was used to conduct parametric study and optimization of PEMFC stack gas purge. The PEMFC stack has 260 cells and an active area of 260 cm<sup>2</sup> per cell. The anode channel was fed with H<sub>2</sub> while the cathode channel was fed with air. Geometric and physical parameters of the PEMFC stack are listed in Table 2. The initial water saturation were set as 0.02 (i.e., 2% of the volume of pores and void space filled with liquid water) in anode GDL and CL and 0.12 in cathode GDL and CL, while membrane water content was in equilibrium with water activity of membrane/GDL interface. Through analyzing the heat capacity of the stack and the latent heat of water evaporation, it was found that the average

**Table 2**  
Geometric and physical parameters.

Parameters	Value
GDL thickness, $\delta_{GDL}$	215 $\mu\text{m}$
Porosity of GDL, $\epsilon$	0.6
CL thickness, $\delta_{CL}$	6.9 $\mu\text{m}$
Porosity of CL, $\epsilon_{CL}$	0.28
Volume fraction of ionomer in CL, $\epsilon_{m}$	0.26
Membrane thickness, $\delta_{mem}$	18 $\mu\text{m}$
Cell length, $L_{cell}$	268 mm
Bipolar plate thickness	0.1 mm
Cathode gas channel width, $w_{chan}$	0.9 mm
Cathode land width, $w_{land}$	1.3 mm
Anode gas channel width, $w_{chan,a}$	1.2 mm
Anode land width, $w_{chan,a}$	1.0 mm
Gas channel depth, $\delta_{chan}$	0.4 mm
Bruggemann factor, $n$	2
Dry membrane density, $\rho_{dry}$	1980 kg/m <sup>3</sup>
Equivalent weight of membrane, $EW$	1.1
Water vapor diffusivity in H <sub>2</sub> , $D_{g,H_2}^w$	$9.15 \times 10^{-5} \text{ m}^2/\text{s}$
Water vapor diffusivity in air, $D_{g,air}^w$	$2.56 \times 10^{-5} \text{ m}^2/\text{s}$

temperature of the stack decreased only 1.4 °C if all water in the stack evaporated. Therefore, in this study, the effect of evaporation heat was negligible and the gas purge process can be perceived as isothermal.

#### 4.1. Grid independency

A typical purge condition was chosen for grid independency test. Details of the purge condition are listed in Table 3.

Variation of HFR with time, which is also called purge curve, was used for grid dependency test. Fig. 4(a) depicts purge curves corresponding to different grid numbers in the flow direction with time step of 0.2 s (The simulation results showed that time step of 0.2 s is small enough, which will be discussed later). No apparent disparity can be observed among purge curves when grid number is larger than 60, indicating that solutions with grid number beyond this value are independent of grid number. In this study, grid number of 100 along the flow direction was selected. Fig. 4 (b) shows the purge curves corresponding to different time steps with grid number of 100. Difference among purge curves was slight when time step was smaller than 1.0 s. In consideration of solution accuracy and time expense, a time step of 0.2 s was chosen.

#### 4.2. Parametric effects

Fig. 5(a) shows the effect of cathode inlet relative humidity on the purge performance. It can be observed that a lower relative humidity accelerates gas purge process. The effect of the relative humidity can be attributed to two aspects. On one hand, a lower relative humidity provides larger vapor concentration gradient between GDL and gas channel, thus enhancing vapor diffusion. On the other hand, purge stream with a lower relative humidity has larger capacity for carrying water vapor out of fuel cell at the same temperature.

Fig. 5(b) displays purge curves for various flow rates. It is shown that gas purge with high flow rate exhibits better performance. A larger flow rate increases the water removal rate from the gas channel and thereby improves purge effectiveness.

Based on the assumption that water removal is driven by vapor-phase transport, the purge performance is expected to be strongly dependent on saturated vapor pressure or equivalently, cell temperature. Fig. 5(c) gives the variation of membrane HFR with time for different cell temperature. It can be seen that HFR rise becomes earlier and faster when temperature increases. Saturated vapor pressure increases with an increase in temperature. As a result, more water vapor can be carried away by purge stream at a higher cell temperature, leading to a higher water removal rate. Moreover, high temperature enhances diffusivity of vapor in GDL and thus renders a larger water flux into channel, which also contributes to better purge performance.

The purge curves for different flow configurations are shown in Fig. 5(d). Gas purge in counter-flow is slower than in co-flow. Fig. 5 (e) shows the relative humidity distribution along the anode and cathode gas channel at different time instance for the counter-flow. Zero distance represents cathode inlet and anode outlet. A declination of relative humidity near anode outlet can

**Table 3**

Purge condition for grid independency test.

Purge conditions	Value
Cell temperature	60 °C
Flow configuration	Co-flow
Cathode flow rate	$1.3 \times 10^{-6} \text{ m}^3/\text{s}$
Anode flow rate	$1.3 \times 10^{-6} \text{ m}^3/\text{s}$
Cathode relative humidity	40%
Anode relative humidity	0%

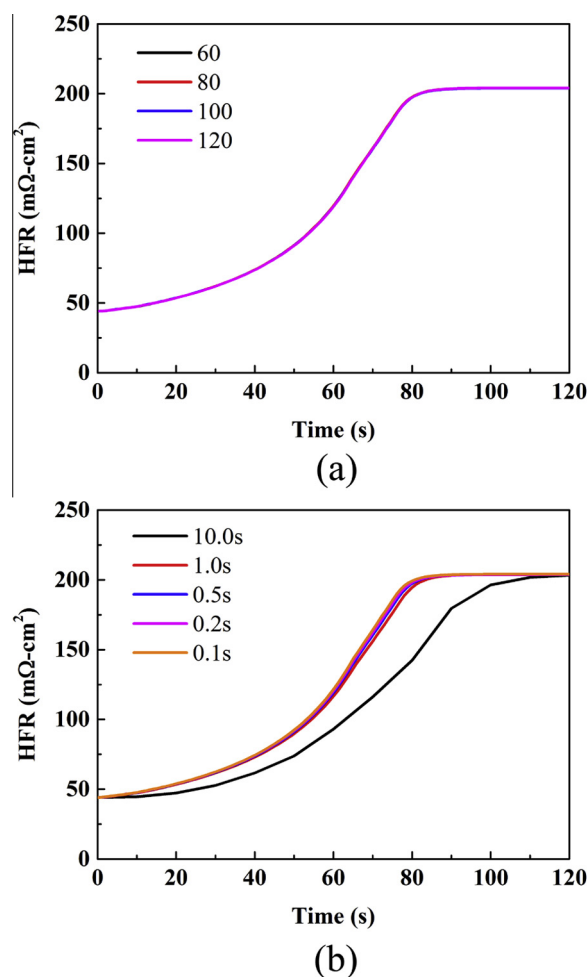


**Fig. 4.** Variation of membrane HFR with time for (a) different grid numbers and (b) different time steps.

be observed, demonstrating that part of water vapor is absorbed by membrane. It is very likely that this part of water vapor transports through the membrane and enters into the cathode purge stream, reducing water removal capacity of cathode purge gas. A similar phenomenon can also be found at the cathode outlet, as shown in Fig. 5(f), which gives rise to a kind of water recirculation. Due to the water recirculation, less water can be purged out of the cell so that the purge performance for the counter-flow is worse. It is interesting to note that water recirculation during the counter-flow gas purge has been the common sense in the fuel cell engineering for all operations. This once again shows the feasibility of our physical and numerical model.

#### 4.3. Purge protocols

In order to improve purge performance, several purge protocols are proposed and discussed for the PEMFC of SAIC. Both purge effectiveness and energy consumption are taken into account for the evaluation of purge performance. Purge effectiveness refers to the purge time that is required for HFR to reach equilibrium. In this study, HFR is considered to be equilibrium if HFR remains unchanged for more than 5 s. During gas purge, energy is mainly consumed by air compressor and heaters for pumping and heating purge gas, respectively. However, since it is rather difficult to calculate the pumping energy, only energy

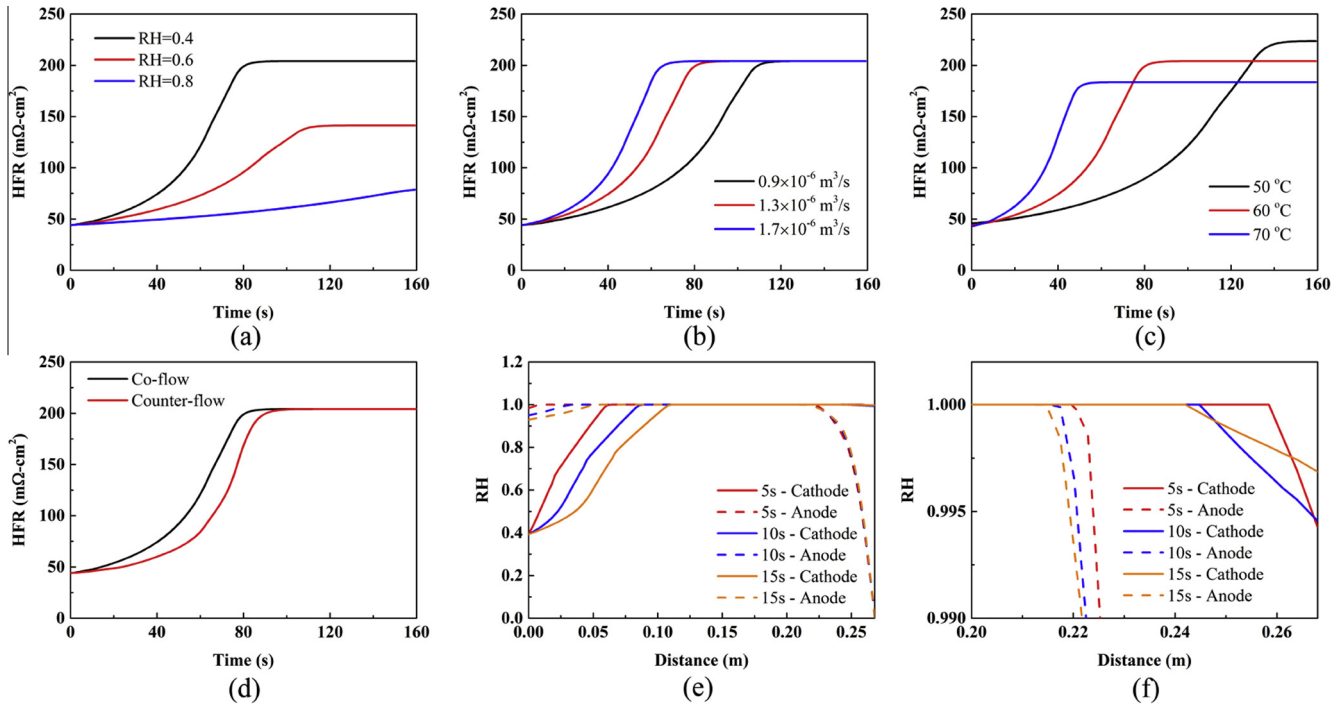


**Fig. 5.** Variation of membrane HFR with time for (a) various inlet relative humidity (b) various flow rates (c) various cell temperatures and (d) different flow configurations. (e) Relative humidity along the gas channel of cathode and anode for counter-flow. (f) Decline of relative humidity near cathode outlet for counter-flow.

for heating is taken into account with an ambient temperature of 25 °C. After shutdown, the power for humidifier was cut off. However, in the fuel cell system designed by SAIC, air went through the humidifier before entering the cathode. According to the experimental data provided by SAIC, the relative humidity of air at cathode inlet was kept around 90% for several minutes after shutdown. Therefore, the cathode inlet humidity is set to be 90% for all protocols.

Fig. 6 gives the purge times for different flow rates and temperatures. For every case shown in Fig. 6, anode flow rate is the same as cathode flow rate. It can be seen that the purge times decrease with an increase in flow rate at three temperatures. So far, there isn't any published criteria on gas purge time for PEMFC vehicle. Here, the authors proposed that the purge time should be shorter than 300 s, otherwise it would be too long for the driver to wait after shutdown. It can be seen that gas purge at 70 °C can easily meet this requirement with a small flow rate.

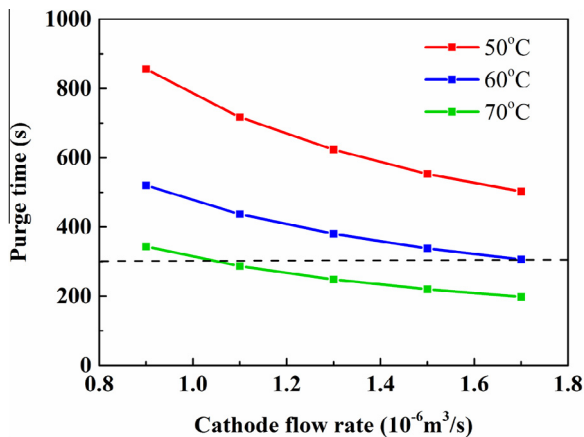


**Fig. 6.** Variation of purge time with flow rate for different cell temperatures.

Then, the cell temperature was fixed at 70 °C and the effect of flow rate was tested. Fig. 7(a) shows the purge times for different flow rates of anode and cathode. Gas purge cases, whose purge times are shorter than 300 s, are surrounded by a dashed box. Corresponding energy consumptions, which are normalized by the active area (260 cm<sup>2</sup>), are shown in Fig. 7(b). As we can see, the purge protocol with cathode flow rate of  $1.5 \times 10^{-6}$  m<sup>3</sup>/s and anode flow rate of  $0.75 \times 10^{-6}$  m<sup>3</sup>/s is the most energy-saving among all protocols in the dashed box. Therefore, this purge protocol is selected as the optimal one. The purge time for the optimal purge is 270 s and the energy consumption is 5.50 J/cm<sup>2</sup>.

Membrane water content is also of great importance due to its significant effect on cold start [25]. The average membrane water content after gas purge are depicted in Fig. 8. Membrane water contents for different anode flow rates are so close to each other that only one curve can be seen. It is shown that the flow rate has little effect on membrane water content, when HFR reaches equilibrium. The average membrane water content for the optimal purge protocol is 7.8, which is important and should be considered in the cold-start strategy design.

## 5. Conclusions

In this study, a purge model to investigate water transport phenomena during gas purge was developed. A comparison between the simulated and experimental results was performed to validate of this model. Based on our model, numerical simulations were implemented to study the effects of various purge conditions on purge performance. Water recirculation was found during the counter-flow gas purge in our numerical simulation and it rendered worse purge performance. Furthermore, purge protocols were optimized under the consideration of purge effectiveness and energy consumption.

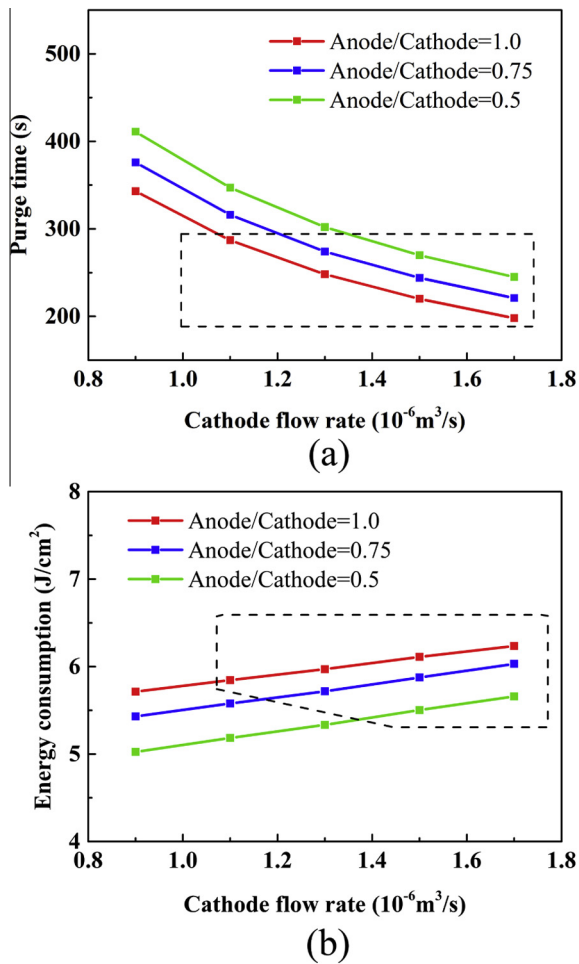


Fig. 7. Variation of (a) purge time and (b) energy consumption with cathode flow rate for different anode flow rates.

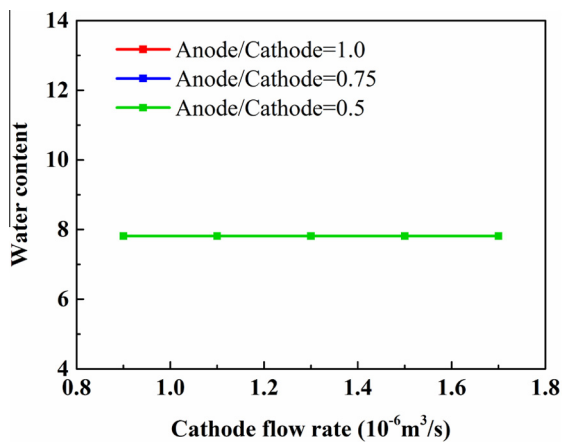


Fig. 8. Variation of water content with cathode flow rate for different anode flow rates.

## Acknowledgements

This research was supported by the National Natural Science Foundation of China (Grant No. 51136004) and the National Key Basic Research Program of China (973 Program) (Grant No. 2013CB228304).

## References

- [1] R. O'Hayre, S.-W. Cha, W. Colella, F.B. Prinz, *Fuel Cell Fundamentals*, John Wiley & Sons, 2009.
- [2] Z. Wan, H. Chang, S. Shu, Y. Wang, H. Tang, A review on cold start of proton exchange membrane fuel cells, *Energies* 7 (5) (2014) 3179–3203.
- [3] F. Jiang, W. Fang, C.-Y. Wang, Non-isothermal cold start of polymer electrolyte fuel cells, *Electrochim. Acta* 53 (2) (2007) 610–621.
- [4] K. Tajiri, C.Y. Wang, Y. Tabuchi, Water removal from a PEFC during gas purge, *Electrochim. Acta* 53 (2008) 6337–6343.
- [5] S. Ge, C.Y. Wang, Characteristics of subzero startup and water/ice formation on the catalyst layer in a polymer electrolyte fuel cell, *Electrochim. Acta* 52 (2007) 4825–4835.
- [6] C.Y. Lee, Y.M. Lee, S.J. Lee, Local area water removal analysis of a proton exchange membrane fuel cell under gas purge conditions, *Sensors* 12 (2012) 768–783.
- [7] S.-Y. Lee, S.-U. Kim, H.-J. Kim, J.H. Jang, I.-H. Oh, E.A. Cho, S.-A. Hong, J. Ko, T.-W. Lim, K.-Y. Lee, T.-H. Lim, Water removal characteristics of proton exchange membrane fuel cells using a dry gas purging method, *J. Power Sources* 180 (2) (2008) 784–790.
- [8] P.K. Sinha, P. Halleck, C.-Y. Wang, Quantification of liquid water saturation in a PEM fuel cell diffusion medium using X-ray microtomography, *Electrochem. Solid-State Lett.* 9 (7) (2006) A344–A348.
- [9] J. St-Pierre, A. Wong, J. Diep, D. Kiel, Demonstration of a residence time distribution method for proton exchange membrane fuel cell evaluation, *J. Power Sources* 164 (1) (2007) 196–202.
- [10] K.T. Cho, M.M. Mench, Fundamental characterization of evaporative water removal from fuel cell diffusion media, *J. Power Sources* 195 (12) (2010) 3858–3869.
- [11] K.T. Cho, M.M. Mench, Effect of material properties on evaporative water removal from polymer electrolyte fuel cell diffusion media, *J. Power Sources* 195 (19) (2010) 6748–6757.
- [12] K.T. Cho, M.M. Mench, Coupled effects of flow field geometry and diffusion media material structure on evaporative water removal from polymer electrolyte fuel cells, *Int. J. Hydrogen Energy* 35 (22) (2010) 12329–12340.
- [13] H.Y. Tang, A. Santamaria, J.W. Park, C. Lee, W. Hwang, Quantification of water in hydrophobic and hydrophilic flow channels subjected to gas purging via neutron imaging, *J. Power Sources* 196 (22) (2011) 9373–9381.
- [14] J.P. Owejan, J.J. Gagliardo, S.R. Falta, T.A. Trabold, Accumulation and removal of liquid water in proton exchange membrane fuel cells, *J. Electrochem. Soc.* 156 (12) (2009) B1475–B1483.
- [15] S.I. Kim, N.W. Lee, Y.S. Kim, M.S. Kim, Effective purge method with addition of hydrogen on the cathode side for cold start in PEM fuel cell, *Int. J. Hydrogen Energy* 38 (26) (2013) 11357–11369.
- [16] Y.S. Kim, S.I. Kim, N.W. Lee, M.S. Kim, Study on a purge method using pressure reduction for effective water removal in polymer electrolyte membrane fuel cells, *Int. J. Hydrogen Energy* 40 (30) (2015) 9473–9484.
- [17] P.K. Sinha, C.-Y. Wang, Gas purge in a polymer electrolyte fuel cell, *J. Electrochem. Soc.* 154 (11) (2007) B1158–B1158.
- [18] H. Ito, T. Maeda, A. Kato, T. Yoshida, Ø. Ulleberg, Gas purge for switching from electrolysis to fuel cell operation in polymer electrolyte unitized reversible fuel cells, *J. Electrochem. Soc.* 157 (7) (2010) B1072–B1080.
- [19] P.K. Sinha, C.-Y. Wang, Two-phase modeling of gas purge in a polymer electrolyte fuel cell, *J. Power Sources* 183 (2) (2008) 609–618.
- [20] M. Khandelwal, S. Lee, M.M. Mench, Model to predict temperature and capillary pressure driven water transport in PEFCs after shutdown, *J. Electrochem. Soc.* 156 (2009), B703–B703.
- [21] X. Wang, K. Tajiri, R.K. Ahluwalia, Water transport during startup and shutdown of polymer electrolyte fuel cell stacks, *J. Power Sources* 195 (19) (2010) 6680–6687.
- [22] S. Ge, C.-Y. Wang, In Situ imaging of liquid water and ice formation in an operating PEFC during cold start, *Electrochem. Solid-State Lett.* 9 (2006), A499–A499.
- [23] C.Y. Lee, Y.M. Lee, S.J. Lee, Local area water removal analysis of a proton exchange membrane fuel cell under gas purge conditions, *Sensors* 12 (1) (2012) 768–783.
- [24] K. Tajiri, Y. Tabuchi, F. Kagami, S. Takahashi, K. Yoshizawa, C.-Y. Wang, Effects of operating and design parameters on PEFC cold start, *J. Power Sources* 165 (1) (2007) 279–286.
- [25] K. Tajiri, Y. Tabuchi, C.-Y. Wang, Isothermal cold start of polymer electrolyte fuel cells, *J. Electrochem. Soc.* 154 (2) (2007), B147–B147.
- [26] P.K. Sinha, C.-Y. Wang, Gas purge in a polymer electrolyte fuel cell, *J. Electrochem. Soc.* 154 (2007) B1158.
- [27] R. Bird, W. Stewart, E. Lightfoot, *Transport Phenomena*, John Wiley & Sons, New York, 1960.
- [28] S. Ge, X. Li, B. Yi, I.M. Hsing, Absorption, desorption, and transport of water in polymer electrolyte membranes for fuel cells, *J. Electrochem. Soc.* 152 (6) (2005) A1149–A1157.
- [29] P. Berg, K. Promislow, J.S. Pierre, J. Stumper, B. Wetton, Water management in PEM fuel cells, *J. Electrochem. Soc.* 151 (3) (2004), A341–A341.
- [30] T.A. Zawodzinski, Water Uptake by and Transport Through Nafion® 117 Membranes, *J. Electrochem. Soc.* 140 (4) (1993) 1041–1047.

- [31] J.T. Hinatsu, Water uptake of perfluorosulfonic acid membranes from liquid water and water vapor, *J. Electrochem. Soc.* 141 (6) (1994) 1493–1498.
- [32] T.E. Springer, T.A. Zawodzinski, S. Gottesfeld, Polymer electrolyte fuel cell model, *J. Electrochem. Soc.* 138 (8) (1991) 2334–2342.
- [33] H. Ju, C.-Y. Wang, S. Cleghorn, U. Beuscher, Nonisothermal modeling of polymer electrolyte fuel cells: I. Experimental validation, *J. Electrochem. Soc.* 152 (8) (2005) A1645–A1653.
- [34] K. Jiao, X. Li, Three-dimensional multiphase modeling of cold start processes in polymer electrolyte membrane fuel cells, *Electrochim. Acta* 54 (27) (2009) 6876–6891.